Research on Chemical Intermediates (2019) 45:5111–5124
https://doi.org/10.1007/s11164-019-03880-7

Nitrogen-doped $ZnWO_4$ nanophotocatalyst: synthesis, characterization and photodegradation of methylene blue under visible light

Mahbobeh Rahmani[1] · **Tahereh Sedaghat**[1]

Received: 19 February 2019 / Accepted: 5 June 2019 / Published online: 12 June 2019

Abstract

Nitrogen-doped $ZnWO_4$ nanoparticles have been synthesized by a sol–gel method using sodium tungstate and zinc acetate in the presence of urea to supply nitrogen. This photocatalyst was characterized by X-Ray diffraction (XRD), field emission-scanning electron microscopy (FESEM), transmission electron microscopy (TEM), an energy dispersive X-ray spectrometer (EDS), the Brunauer–Emmett–Teller technique (BET), photoluminescence (PL) spectroscopy and UV–vis diffuse–reflectance spectrum (DRS). The band gap energy of N-doped $ZnWO_4$ was about 2.99 eV and the absorption wavelength shifted to the visible region in comparison to pure $ZnWO_4$. Also, N-doped catalyst shows enhanced photocatalytic activity for the degradation of methylene blue (MB). The apparent photodegradation rate constant (k) of N-doped $ZnWO_4$ was observed 3.57×10^{-2} min^{-1} under visible light irradiation.

Keywords $ZnWO_4$ · Nitrogen doping · Photocatalyst · Methylene blue

Introduction

The improvement of the photocatalytic activity of the wide band gap semiconductors, such as TiO_2, ZnO, $ZnWO_4$ and CuO, for practical applications under visible light, has been very much considered [1–6]. This is due to the fact that visible light with the wavelength between 400 and 700 nm constitutes about 45% and the UV light is less than 10% of the solar radiation energy $ZnWO_4$ as a member of the tungstate family has been used to mineralize organic pollutants under UV light irradiation, but its photocatalytic activity is not high enough. The scientists tried to solve this disadvantage by nonmetal or transition metals doping [7–12] or coupling of semiconductors [5, 13–17]. For instance, introduction of fluorine into the

✉ Tahereh Sedaghat
tsedaghat@scu.ac.ir

[1] Department of Chemistry, Faculty of Science, Shahid Chamran University of Ahvaz, Ahvaz, Iran

$ZnWO_4$ improves photocatalytic activity for F–$ZnWO_4$ under UV light irradiation [18]. Guangli et al. synthesized chlorine-doped $ZnWO_4$ photocatalysts by the hydrothermal process. In this way, the band gap energy of $ZnWO_4$ decreased to 3.68 eV [19]. Also, Song et al. [11] synthesized Cd-doped $ZnWO_4$ nanorods by the hydrothermal method. Their experiments showed the best activity in photodegradation of RhB in aqueous solution under UV light illumination. Li and Co-doping of $ZnWO_4$ enhanced the band gap to 3.55 and 3.23 eV, respectively, and doped photocatalysts were used for the degradation of rhodamine B by the irradiation [20, 21]. Also, Dutta and Raval [8] studied the effect of transition metal ion (Cr^{3+}, Mn^{2+} and Cu^{2+}) doping on photocatalytic activity of the doped $ZnWO_4$ nanoparticles under visible light irradiation.

Doping with transition metals has some problems, such as thermal instability and increasing of charge carrier recombination centers; thus their application is limited for photocatalytic reactions [18, 22, 23]. On the other hand, doping of nonmetal anions in the semiconductors has been proven to be very promising for efficient photocatalytic oxidation of organic compounds under visible light radiation [18, 24, 25]. In order to have a red shift of the $ZnWO_4$ absorption edge, the anions should have a higher p orbital energy than O 2p, and they should be weaker electronegatively than the O atom [18]. Nitrogen is known as an effective dopant because the ionic radii of nitrogen and oxygen are comparable, and the mixing of 2p levels of oxygen and nitrogen decreases significantly the energy gap of the photocatalysts [26].

Here, to continue our previous work [27], we decided to synthesized N-doped $ZnWO_4$ by a simple sol–gel method. Our aim is to obtain a photocatalyst with better performance than the pure $ZnWO_4$, i.e., high photoactivity under visible light and good recycling performance. We will compare the performance of this new catalyst in the degradation of methylene blue (MB) dye with the pure $ZnWO_4$ in the same conditions [27].

Experimental

Materials

All the chemicals used in this study, zinc acetate [$Zn(CH_3CO_2)_2{\cdot}2H_2O$, assay 99.5%], sodium tungstate ($Na_2WO_4{\cdot}2H_2O$, assay 99%), ammonia (25 wt% NH_3), hydrocholoric acid (37–40 wt% HCl), ethanol (assay 99.7–100%), methylene blue and urea were of analytical grade and used without further purification. All aqueous solutions were prepared by using deionized water. Pure $ZnWO_4$ nanoparticles were synthesized by a facile sol–gel method according to a procedure we reported earlier [27].

Characterization methods

X-ray diffraction (XRD) data were collected from powder samples using a Philips PW1730 diffractometer with monochromatic Cu Kα radiation ($\lambda = 0.15406$ nm)

in the 2θ range from 10° to 80°. The field emission-scanning electron microscopy (FESEM) images were taken by a MIRA3 TESCAN microscope at an accelerating voltage of 15 kV together with an energy dispersive X-ray (EDX) for analysis of the elements composition of samples. Transmission electron microscopy (TEM) images was carried out using an FM10C-100 kV series microscope (Zeiss company Germany). The UV–vis diffuse–reflectance spectra (DRS) were recorded using a Shimadzu (MPC -2200) Spectrophotometer in the range of 200–1100 nm to evaluate the band gap energy of samples. The Brunauer–Teller (BET) surface area of the products was measured by micromeritics (Gemini). Photoluminescence (PL) emission spectra of the samples were measured using Avaspec 2048 TEC with a 450 W xenon lamp.

Synthesis of N-doped $ZnWO_4$ photocatalyst

Nanosized N-doped $ZnWO_4$ photocatalyst was prepared by using the sol–gel method. A solution containing 30 mL ethanol and 3 mL HCl was dropwise added into a mixture of zinc acetate (0.025 mol) in ethanol (40 mL) under vigorous stirring. The obtained suspension was ultrasonicated for 30 min to dissolve zinc acetate completely. Then a solution of $Na_2WO_4{\cdot}2H_2O$ (0.025 mol) in deionized water (20 mL) was added dropwise under vigorous stirring. After that, 0.10 mol urea (6.2 g) at a Zn:urea molar ratio of 1:4 was dissolved in a solution of absolute ethanol and deionized water (4:1, 60 mL). This urea solution was added dropwise into a previous mixture under intensive stirring. The reaction mixture was stirring for 4 h continuously and the resulting colloidal suspension was aged for 48 h in room temperature until the formation of xerogel. The gel was filtered, washed with a solution of ethanol and deionized water (4:1) for several times and dried in air at 80 °C for 2 h. The dried gel was calcined at 500 °C for 5 h under a heating rate of 10 °C min^{-1}. Finally, the product was ground in an agate mortar to achieve a fine powder.

Photocatalytic experiments

The photocatalytic activity of N-doped $ZnWO_4$ nanoparticles was evaluated by photodegradation of methylene blue (MB) aqueous solution at room temperature. The photoreactor was equipped with an 18 W fluorescent lamp (NARVA, LT 18W/0182 blue, Germany) for visible light illumination ($\lambda = 400$–600 nm). Photocatalyst nanoparticles (0.2 g) were dispersed in 100 mL of 16 mg L^{-1} MB aqueous solution. These suspensions were magnetically stirred in the dark for 1 h to set up adsorption–desorption equilibrium before illumination. The concentration of the dye after adsorption was taken as the initial concentration of the pollutant. Then, the solution was irradiated under magnetic stirring. The lamp was positioned 10 cm above from the surface of the suspensions. The change in the concentration of the dye was detected using the UV–vis spectrophotometer. In this way, 3 mL of solution was taken out at regular irradiation time intervals (each 30 min), and it was centrifuged at 5000 rpm for 20 min to obtain the clear solution. The concentration of

remaining dye in collected solution was monitored by measuring the absorbance of the extracted solution at 664 nm in a quartz cell.

Results and discussion

Characterization

Figure 1 shows the XRD pattern of N-doped $ZnWO_4$ in comparison to pure $ZnWO_4$ previously reported [27]. The 2θ values corresponding to pure $ZnWO_4$ (JCPDS card no. 15-0774) are 23.93°, 24.67°, 30.53°, 31.35°, 36.48°, 38.48°, 41.41°, 44.76°, 46.04°, 48.83°, 50.37°, 51.80°, 53.75°, 54.30°, 58.58°, 61.88°, 65.59° and 68.32° that match the respective (011), (110), (111), (020) (002), (200) (121), (112), (211), (022), (220), (130), (202), (221), (013), (113), (311) and (041) planes of monoclinic $ZnWO_4$ [28]. Therefore, N-doping has not changed the crystalline structure of $ZnWO_4$. There are a number of additional peaks in this XRD pattern related to $Na_2W_2O_7$ (JCPDS card no. 98-000-0983) and $Na_2W_4O_{13}$ (JCPDS card no. 98-000-2045) phases, for which their formation in the acidic environment is inevitable [27].

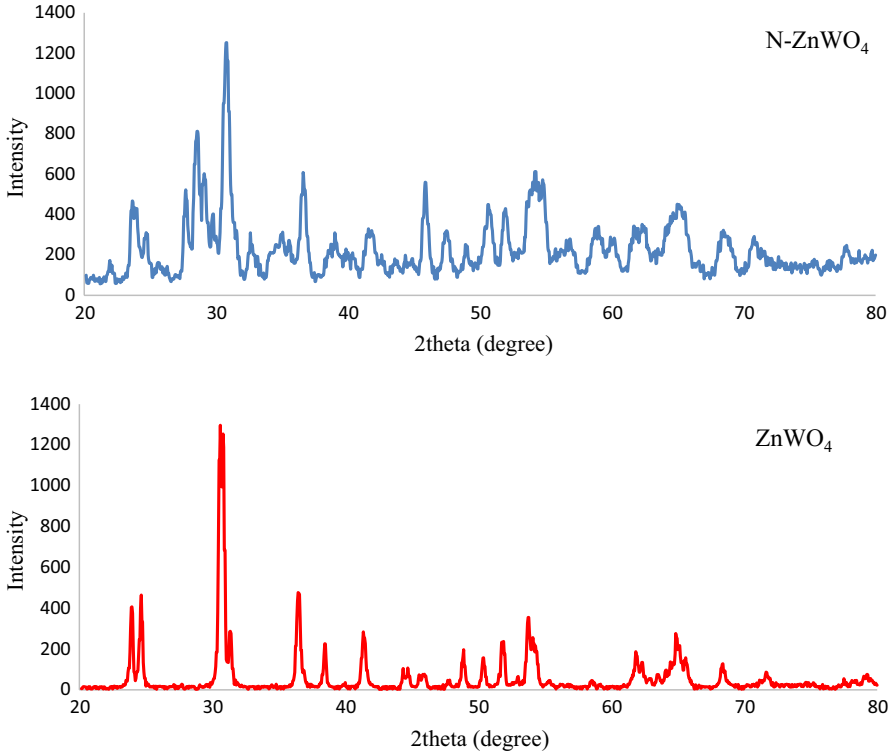

Fig. 1 XRD patterns of the $ZnWO_4$ [21] and N-doped $ZnWO_4$ obtained bythe sol–gel procedure

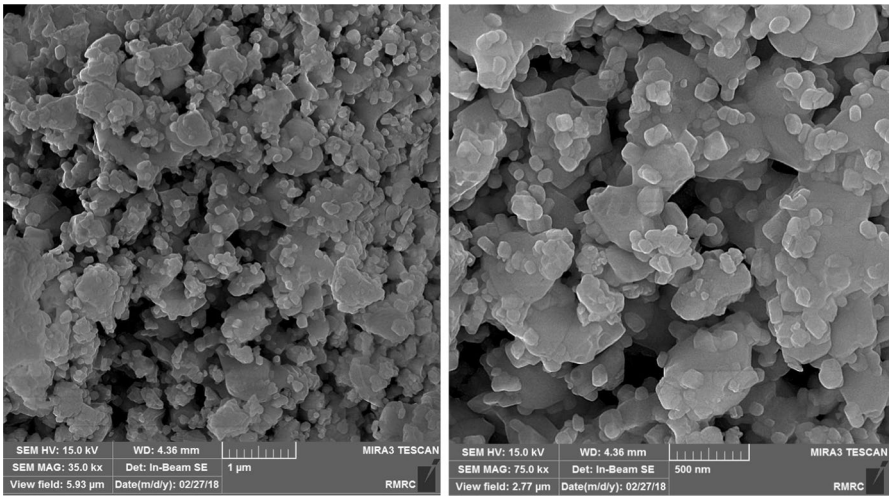

Fig. 2 FESEM images of N-doped $ZnWO_4$ nanoparticles

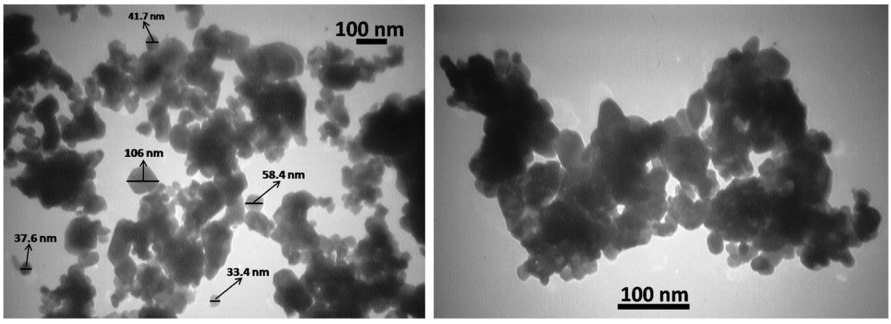

Fig. 3 TEM images of the N-doped $ZnWO_4$ nanoparticles

From the XRD pattern of the N-doped $ZnWO_4$, it can be found that the diffraction peaks slightly shift toward higher angles with the doping of nitrogen. Also, a significant peak broadening was observed, implying a decreasing of crystallinity due to the doping of nitrogen into the $ZnWO_4$. The average crystallite size was estimated for N-doped $ZnWO_4$ by applying the Scherrer's formula ($D = 0.9\lambda/\beta\cos\theta$) on the highest intensity peak of the diffraction patterns (111). The crystallite size was found to be 42.30 nm for N-doped $ZnWO_4$. It had been obtained at 45.77 nm for $ZnWO_4$ [27].

Morphology and size of N-$ZnWO_4$ nanoparticles have been studied by FE-SEM and TEM. As shown in the FESEM images (Fig. 2), N-doped $ZnWO_4$ particles have an agglomerated morphology, and the particle size is about 37–115 nm. In order to determine the exact size of the N-doped $ZnWO_4$, TEM analysis was used. The TEM images (Fig. 3) show the nanoparticles of the N-doped $ZnWO_4$ have an average diameter about 33–106 nm which are in agreement with FESEM results. Therefore,

in comparison with pure $ZnWO_4$ (26–78 nm) [27], nanoparticle sizes have increased after the nitrogen doping.

EDX analysis was performed to confirm the chemical composition and the presence of nitrogen dopant. The EDX patterns of N-doped $ZnWO_4$ are shown in Fig. 4. The EDX pattern of N-doped $ZnWO_4$ shows existence of nitrogen together with Na, Zn, W and O (N 1.26, O 15.87, Na 3.19, Zn 6.53, W 73.15%), demonstrating the successful doping of nitrogen in the $ZnWO_4$. Sodium is observed due to formation of $Na_2W_2O_7$ and $Na_2W_4O_{13}$ phases with $ZnWO_4$ phase in acidic pH [27]. The presence and distribution of elements were visualized by EDX mapping in Fig. 5. This figure clearly shows the uniform doping of nitrogens in $ZnWO_4$.

The nitrogen adsorption–desorption isotherm of N-doped $ZnWO_4$ is shown in Fig. 6. The specific BET surface areas and pore volume of N-doped $ZnWO_4$ in comparison to pure $ZnWO_4$ [27] are shown in Table 1. On the basis of these data, the pure $ZnWO_4$ have higher specific surface area than N-doped samples. This result is due to smaller size of $ZnWO_4$ nanoparticles. The lower surface area of N-$ZnWO_4$ and the presence of pores with small volume correspond to agglomerate particles as was confirmed by the XRD pattern and SEM images.

UV–vis diffuse reflectance spectrum shown in Fig. 7 was used to determine the band gap energy of N-doped $ZnWO_4$. As can be seen, the N-doped $ZnWO_4$ indicated a stronger absorption than pure $ZnWO_4$ in the UV–vis region. The band gap energies (E_g) of this photocatalyst was calculated by the Kubelka–Munk (K–M) method from a plot of $(\alpha h\nu)^2$ versus photon energies (eV) (Fig. 7, insert) using the following equations [29–31]:

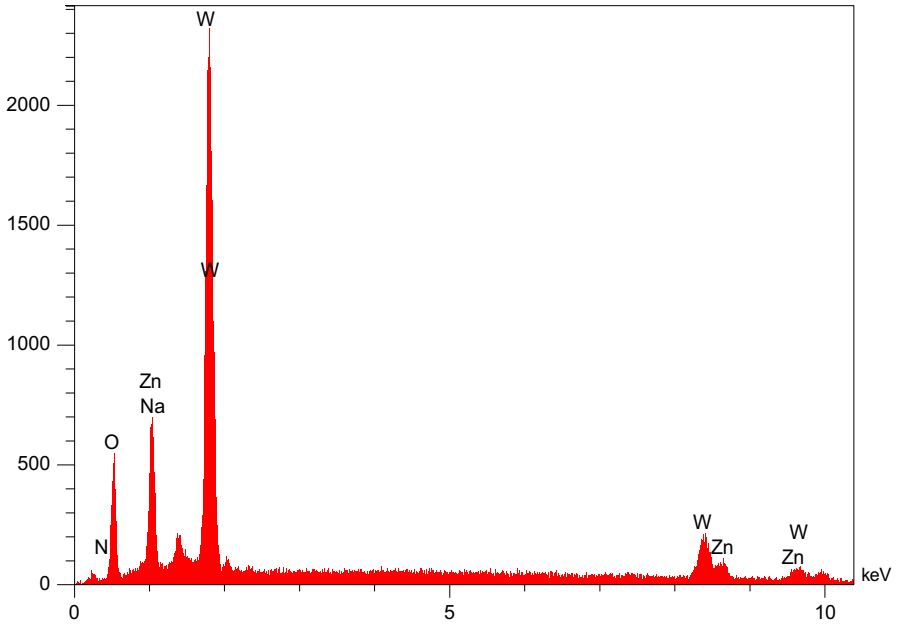

Fig. 4 EDX of the N-doped $ZnWO_4$ nanoparticles

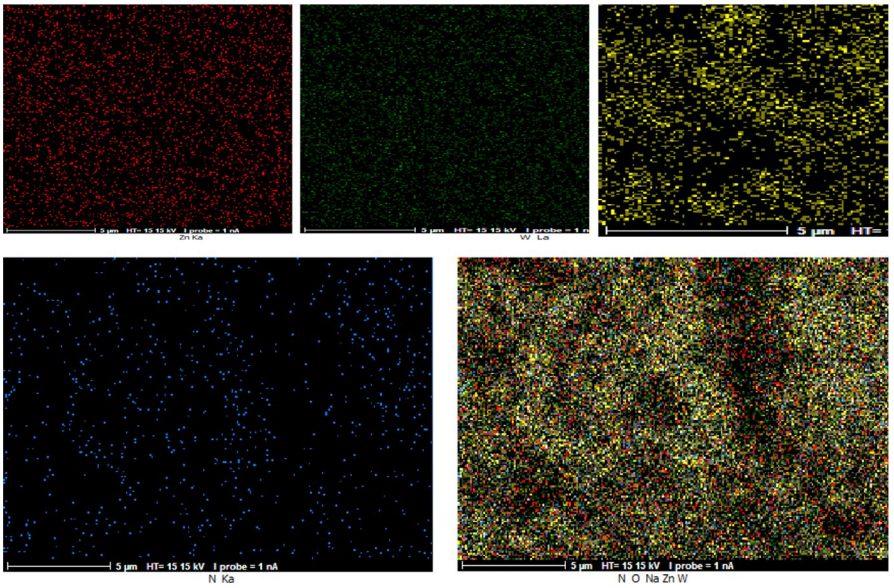

Fig. 5 Elemental mapping of N–$ZnWO_4$; zinc (red), tungsten (green), oxygen (yellow), nitrogen (blue). (Color figure online)

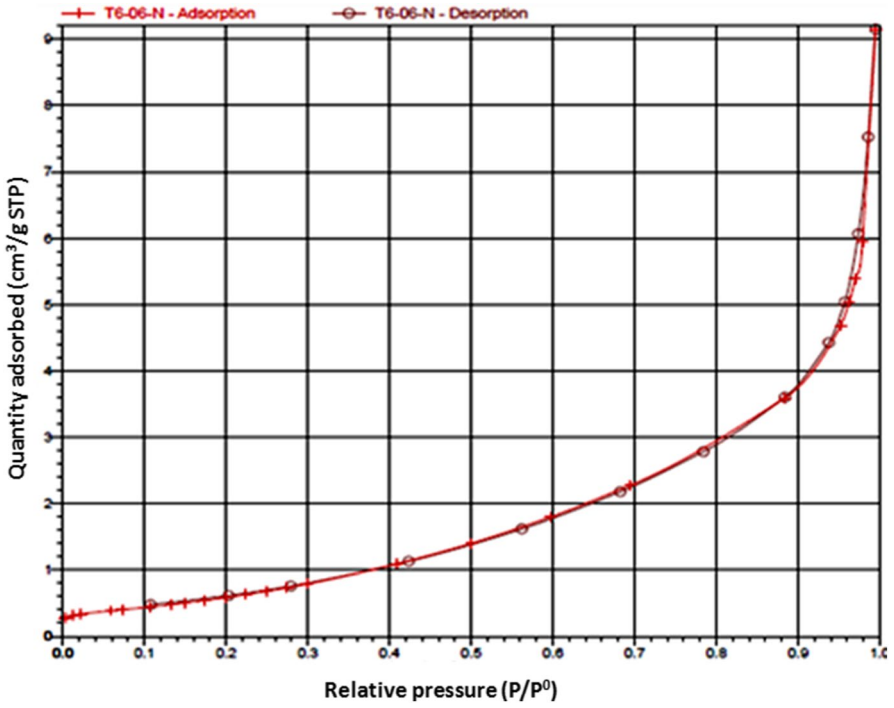

Fig. 6 The nitrogen adsorption–desorption isotherm of N-doped $ZnWO_4$

Table 1 BET surface area of pure and N-doped $ZnWO_4$

Catalyst	BET surface area (m^2/g)	Pore volume (cm^3/g)
N-doped $ZnWO_4$	2.4094	0.007176
$ZnWO_4$	5.5616[a]	0.014570[a]

[a]Reference [21]

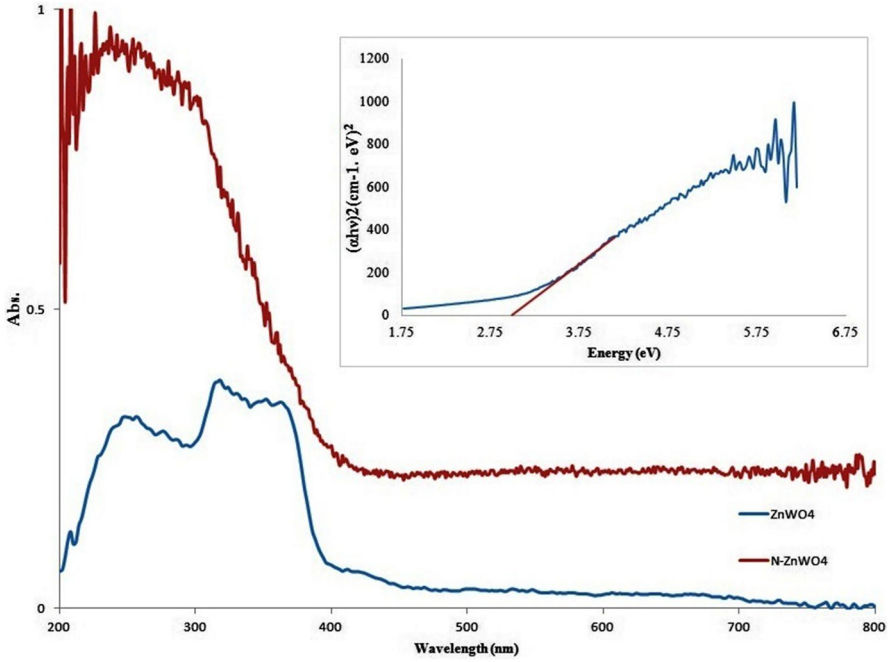

Fig. 7 UV–vis diffuse reflectance absorption spectrum (DRS) of the N-doped $ZnWO_4$ in comparison to $ZnWO_4$ nanoparticles. Insert shows the plot of $(\alpha h\nu)^2$ versus the photon energy (eV) for N–$ZnWO_4$

$$(\alpha h\nu) = A\left(h\nu - E_g\right)^n \quad n = \frac{1}{2}, 2, \frac{3}{2}, 3, \tag{1}$$

$$E = \frac{hc}{\lambda} = \frac{1240}{\lambda}. \tag{2}$$

The bond gap energy can be determined by extrapolation of the linear part of the curve to the $h\nu$ axis intercept that it is calculated to be 2.99 eV. We calculated the band gap of $ZnWO_4$ previously prepared by the sol–gel method as 3.20 eV [27]. Decreasing of band gap energy in the N-doped $ZnWO_4$ is due to the formation of defect energy levels caused by the substitution of the lattice oxygens by nitrogen atoms that can shift the light absorption to the lower energy through band gap narrowing [32–35].

The recombination rate of photoinduced electron–hole pairs was studied by photoluminescence (PL) analysis to investigate N-doping modification effect. The room temperature photoluminescence emission spectrum of N–$ZnWO_4$ in comparison to $ZnWO_4$ has been shown in Fig. 8. It can be observed that the pure $ZnWO_4$ nanoparticles exhibit a high intensity broad peak in the range of 300–700 nm related to charge transition between the O_{2p} orbitals and the empty d orbitals of the central W^{6+} ions in the WO_6 group [27, 28, 36, 37]. The intensity of the PL spectrum of pure $ZnWO_4$ shows that the recombination rate of the photogenerated electrons and holes is high. However, by nitrogen doping a slight red shift and a sharp decrease in the intensity of this emission peak is observed. Decreasing of the intensity of the PL spectrum of N-doped $ZnWO_4$ suggests that doping has effectively suppressed the recombination of the holes and electrons. Also, a sharp emission peak is observed in 506 nm that is overlapped in pure $ZnWO_4$. The addition of nitrogen does not change the position of this emission peak but a slight increase in its intensity is observed. One explanation is that this emission is an indirect emission which is related to surface vacancy on pure or N-doped $ZnWO_4$ lattice [38].

Photocatalytic performance

The photocatalytic activity of N-doped $ZnWO_4$ was investigated by the photodegradation of methylene blue in aqueous solution under visible light irradiation and compared to the pure $ZnWO_4$. MB is an intensely colored compound used in dyeing textiles and is a common water pollutant. Degradation of this dye is difficult under visible light and is often used as a dye contamination model for the evaluation of photocatalyst activity [39, 40]. MB has an apparent absorbance band at 664 nm, whose intensity significantly decreases with increasing the duration of light irradiation time. Figure 9 shows the spectral change during the photodegradation of MB

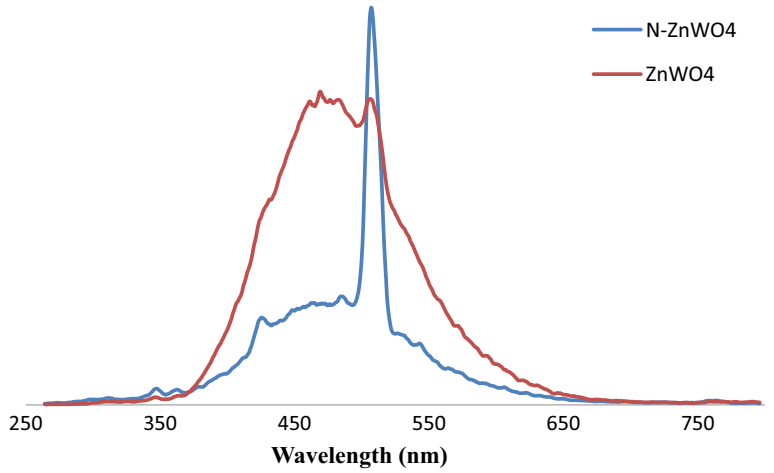

Fig. 8 The room temperature photoluminescence (PL) emission spectra of N-doped $ZnWO_4$ in comparison to $ZnWO_4$

in the presence of N-doped $ZnWO_4$ nanoparticles at various time intervals under irradiation. The most intense absorption band is in accordance with the equilibrium concentration of the MB after 1 h in dark adsorption. The results indicated that the spectral band at 664 nm shifts to shorter wavelength during photodegradation process. These findings are in accordance with the results of Huang [19]. They found that MB degradation occurred via N-demethylation. When all or parts of methyl or methylamine groups are destroyed, the methylene blue color is diminished. Therefore, N-demethylation and oxidative degradation occurs during the photocatalytic decomposition of MB by N-doped $ZnWO_4$ catalysts. Also, the N-doped catalyst shows a good dye adsorption in the dark that it was around 15%. According to the results, the adsorption of the organic compound on the surface of the N-doped $ZnWO_4$ is one of the reaction steps before the photocatalytic reaction occurs at the surface of the catalyst. It might increase the reaction rate of the photodegradation process but it is not enough for the degradation of dye pollutants. Figure 10 shows the photocatalytic degradation of MB solution as a function of irradiation time in the presence of N-doped $ZnWO_4$ in comparison to $ZnWO_4$ nanoparticles. As expected, the photocatalytic efficiency of N-doped sample was higher than that of the pure $ZnWO_4$ and they reached 99.1% and 97.62% degradation after 120 and 240 min, respectively. This results shows that the N-doping decreases the recombination of photogenerated electrons and holes, generates more electron–hole pairs and enhances light harvest capability. Furthermore, adding nitrogen decreases the band gap, and; therefore, enhances the absorption in the visible region. According to the blank test, the photolysis of methylene blue can be ignored.

The photocatalytic degradation rate of MB can be explained by the Langmuir–Hinshelwood (LH) equation:

$$\ln \frac{C_0}{C} = k_{\text{obs}} t, \tag{3}$$

where C_0 is the equilibrium concentration of the MB (mg L^{-1}) after 1 h in dark adsorption and C is the concentration of the MB solution at irradiation time t (min).

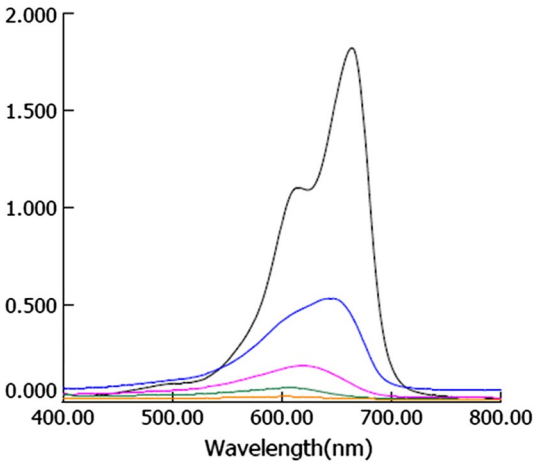

Fig. 9 UV–vis spectral changes of MB aqueous solution by N-doped $ZnWO_4$ under visible light irradiation

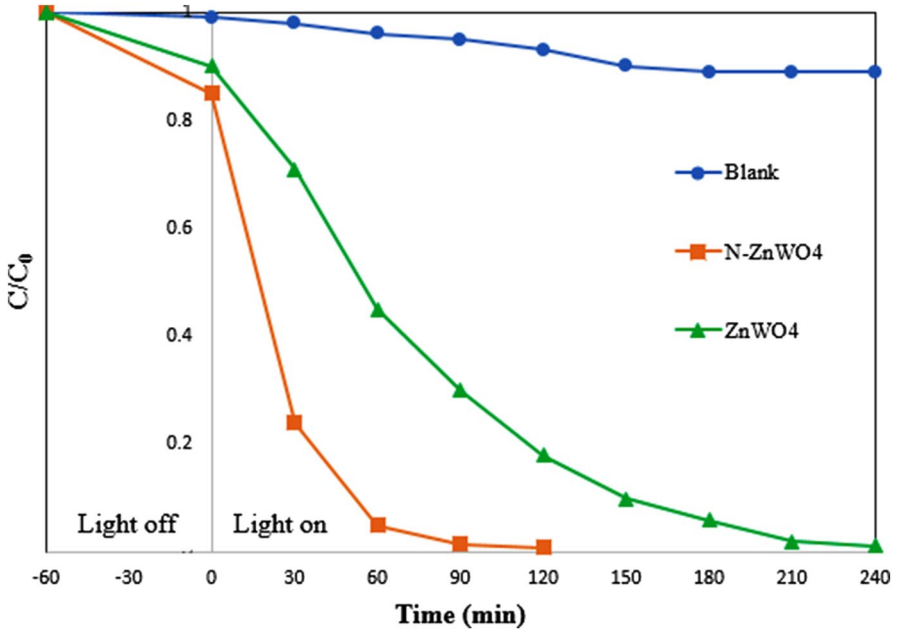

Fig. 10 Photocatalytic degradation of MB in the presence of N-doped $ZnWO_4$ (2 g L^{-1}) in comparison to $ZnWO_4$

The first order linear relationship was observed by the plot of the $\ln(C_0/C)$ versus irradiation time (Fig. 11). From this graph, the observed rate constants of the photodegradation reactions by N-doped $ZnWO_4$ is obtained at 3.75×10^{-2} min^{-1}. This value for the pure $ZnWO_4$ was 1.62×10^{-2} min^{-1} [27]. The results demonstrated that the k value of N-doped $ZnWO_4$ was 2.2 times higher than that of the pure $ZnWO_4$.

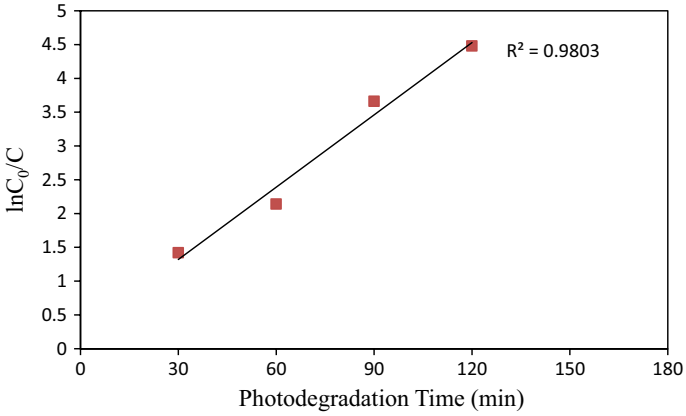

Fig. 11 Photocatalytic kinetics for the degradation of MB by N-doped $ZnWO_4$ under visible light irradiation

Thus the doping of nitrogen created a photocatalyst with improved photocatalytic activity.

The reusability test for MB photodegradation by N-doped $ZnWO_4$ was carried out to investigate the photocatalytic stability of as-prepared catalyst. After every 60 min of photoreaction, the catalyst was separated, washed with deionized water and dried. Figure 12 shows that 95% MB degradation is found in the 1st run of N-doped $ZnWO_4$ which decreases as 90%, 81% and 70% in 2nd, 3rd and 4th run, respectively. Therefore, photodegradation efficiency of N-doped $ZnWO_4$ was still more than 80% after three cycles, and the catalyst did not exhibit any significant loss of activity confirming that as-prepared catalysts are stable during the photocatalytic oxidation of the MB molecules. This reusability results are more desirable than pure $ZnWO_4$ [27]. The structural stability of N–$ZnWO_4$ was also examined by XRD analysis (Fig. 13). The XRD pattern before and after photocatalytic experiment demonstrates the catalysts have good stability and can be recycled without any considerable change in the structure.

Conclusion

The N-doped $ZnWO_4$ nanoparicles were successfully prepared via a simple sol–gel process. In comparison to pure $ZnWO_4$, the band gap energy of N-doped sample reduced to 2.99 eV by the formation of defect energy levels caused by the substitution of the lattice oxygen by nitrogen atoms. Also, the PL experiment validated the high separation of photogenerated charge carriers in the N-doped sample. This

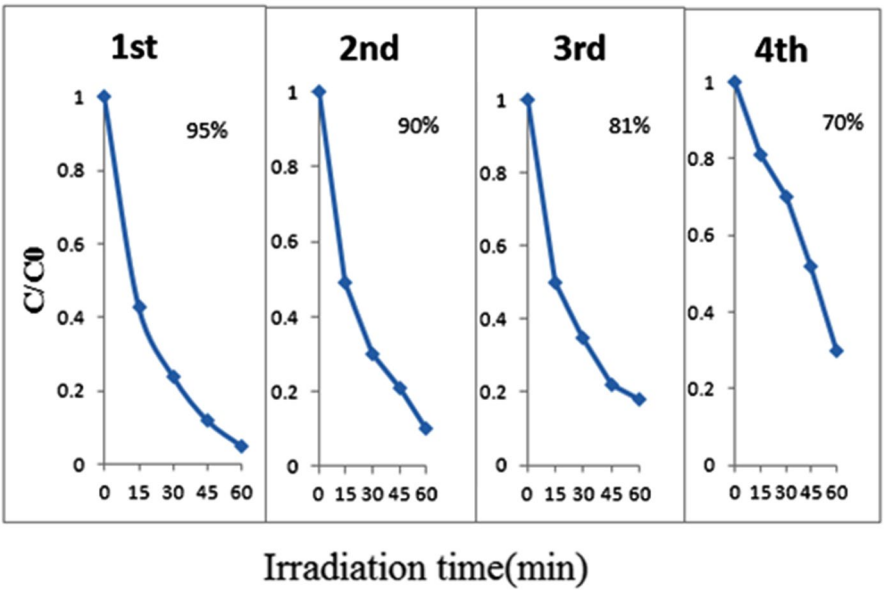

Fig. 12 Cycling runs in the photocatalytic degradation of MB in the presence of N-doped $ZnWO_4$

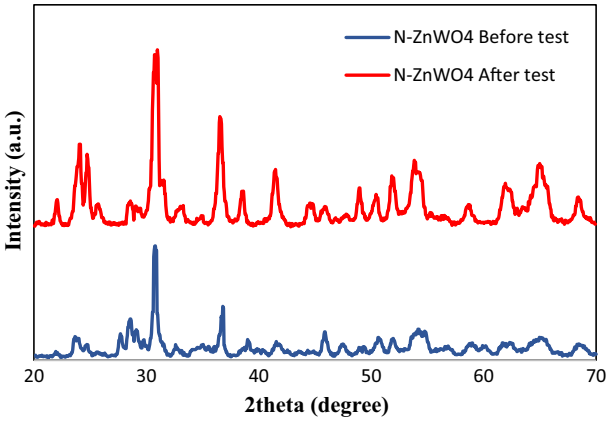

Fig. 13 Comparison of the XRD patterns of N-doped $ZnWO_4$ before and after catalytic tests

N-doped photocatalyst exhibits improved photocatalytic activity and a higher rate constant than pure $ZnWO_4$ for the degradation of the methylene blue under visible light irradiation. The photocatalytic activity of N-doped $ZnWO_4$ decreases only 20% after three successive cycles, confirming that as-prepared catalyst is stable during the photocatalytic oxidation of the MB molecules.

Acknowledgements Support of this work by Shahid Chamran University of Ahvaz, Iran (Grant No. 1397) is gratefully acknowledged.

References

1. M. Daous, V. Iliev, L. Petrov, J. Mol. Catal. A Chem. **392**, 194 (2014)
2. G. Sanzone, M. Zimbone, G. Cacciato, F. Ruffino, R. Carles, V. Privitera, M. Grimaldi, Superlattices Microstruct. **123**, 394 (2018)
3. Q.-Y. Lin, Q. Lin, Y.-Q. Zhang, H.-X. Lin, T.-H. Zhou, S.-B. Ning, X.-X. Wang, Res. Chem. Intermed. **43**, 5067 (2017)
4. M.A. Subhan, P.C. Saha, P. Sarker, M. Al-Mamun, Res. Chem. Intermed. **44**, 6311 (2018)
5. L. Wei, H. Zhang, J. Cao, Mater. Lett. **236**, 171 (2019)
6. H. She, H. Zhou, L. Li, L. Wang, J. Huang, Q. Wang, ACS Sustain. Chem. Eng. **6**, 11939 (2018)
7. Y.-M. Pan, W. Zhang, Z.-F. Hu, Z.-Y. Feng, L. Ma, D.-P. Xiong, P.-J. Hu, Y.-H. Wang, H.-Y. Wu, L. Luo, J. Lumin. **206**, 267 (2019)
8. D.P. Dutta, P. Raval, J. Photochem. Photobiol. A **357**, 193 (2018)
9. Z. Liu, J. Tian, D. Zeng, C. Yu, L. Zhu, W. Huang, K. Yang, D. Li, Mater. Res. Bull. **94**, 298 (2017)
10. A. Phuruangrat, P. Dumrongrojthanath, S. Thongtem, T. Thongtem, Mater. Lett. **166**, 183 (2016)
11. X.C. Song, Y.F. Zheng, E. Yang, G. Liu, Y. Zhang, H.F. Chen, Y.Y. Zhang, J. Hazard. Mater. **179**, 1122 (2010)
12. J. Arin, P. Dumrongrojthanath, O. Yayapao, A. Phuruangrat, S. Thongtem, T. Thongtem, Superlattices Microstruct. **67**, 197 (2014)
13. Q. Wang, Y. Shi, T. Niu, J. He, H. She, B. Su, J. Sol–Gel. Sci. Technol. **83**, 555 (2017)
14. Q. Wang, Y. Shi, Y. Sun, H. She, J. Yu, Y. Yang, New J. Chem. **41**, 1028 (2017)
15. P. Huo, Y. Tang, M. Zhou, J. Li, Z. Ye, C. Ma, L. Yu, Y. Yan, J. Ind. Eng. Chem. **37**, 340 (2016)
16. Y. Wu, J. Tie, C. Chen, N. Luo, D. Yang, W. Hu, X. Liu, Ceram. Int. **45**, 13656 (2019)
17. X. Jiang, X. Zhao, L. Duan, H. Shen, H. Liu, T. Hou, F. Wang, Ceram. Int. **42**, 15160 (2016)

18. L. Sun, X. Zhao, X. Cheng, H. Sun, Y. Li, P. Li, W. Fan, J. Phys. Chem. C **115**, 15516 (2011)
19. G. Huang, Y. Zhu, CrystEngComm **14**, 8076 (2012)
20. G.-T. Xiong, W. Zhang, Z.-F. Hu, P.-J. Hu, Y.-M. Pan, Z.-Y. Feng, L. Ma, Y.-H. Wang, L. Luo, J. Lumin. **206**, 370 (2019)
21. U. Alam, A. Khan, D. Bahnemann, M. Muneer, J. Environ. Chem. Eng. **6**, 4885 (2018)
22. M.I. Litter, Appl. Catal. B **23**, 89 (1999)
23. D. Dvoranova, V. Brezova, M. Mazúr, M.A. Malati, Appl. Catal. B **37**, 91 (2002)
24. R. Asahi, T. Morikawa, T. Ohwaki, K. Aoki, Y. Taga, Science **293**, 269 (2001)
25. S.U. Khan, M. Al-Shahry, W.B. Ingler, Science **297**, 2243 (2002)
26. T. Morikawa, R. Asahi, T. Ohwaki, K. Aoki, Y. Taga, Jpn. J. Appl. Phys. **40**, L561 (2001)
27. M. Rahmani, T. Sedaghat, J. Inorg. Organomet. Polym. **29**, 220 (2019)
28. R. Dai, Z. Wang, Z. Zhang, Z. Ding, Surf. Interface Anal. **46**, 1151 (2014)
29. S.-M. Lam, J.-C. Sin, A.Z. Abdullah, A.R. Mohamed, J. Colloid Interface Sci. **450**, 34 (2015)
30. S. Ebraheem, A. El-Saied, Mater. Sci. Appl. **4**, 324 (2013)
31. H. Fu, J. Lin, L. Zhang, Y. Zhu, Appl. Catal. A **306**, 58 (2006)
32. D. Zhang, J. Gong, J. Ma, G. Han, Z. Tong, Dalton Trans. **42**, 16556 (2013)
33. A.B. Patil, K.R. Patil, S.K. Pardeshi, J. Hazard. Mater. **183**, 315 (2010)
34. L.-C. Chen, Y.-J. Tu, Y.-S. Wang, R.-S. Kan, C.-M. Huang, J. Photochem. Photobiol. A **199**, 170 (2008)
35. M. Batzill, E.H. Morales, U. Diebold, Phys. Rev. Lett. **96**, 026103 (2006)
36. J. Huang, L. Gao, J. Am. Ceram. Soc. **89**, 3877 (2006)
37. M. Hojamberdiev, G. Zhu, Y. Xu, Mater. Res. Bull. **45**, 1934 (2010)
38. C. Zhang, H. Zhang, K. Zhang, X. Li, Q. Leng, C. Hu, A.C.S. Appl, Mater. Interfaces **6**, 14423 (2014)
39. J. Tang, Z. Zou, J. Yin, J. Ye, Chem. Phys. Lett. **382**, 175 (2003)
40. A. Houas, H. Lachheb, M. Ksibi, E. Elaloui, C. Guillard, J.-M. Herrmann, Appl. Catal. B **31**, 145 (2001)